

AD-A282644

FIRST PRINCIPLES INVESTIGATION OF THE  
Ir-Zr-Nb TERNARY SYSTEM

**DTIC**  
**S** ELECTE  
JUL 28 1994  
**F**

by

GREGORY A. MILLER, B.S.

N00014-90-J-1185

THESIS

Presented to the Faculty of the Graduate School of  
The University of Texas at Austin  
in Partial Fulfillment  
of the Requirements  
for the Degree of  
MASTER OF SCIENCE IN ENGINEERING

This document has been approved  
for public release and sale; its  
distribution is unlimited.

THE UNIVERSITY OF TEXAS AT AUSTIN

May 1994

DTIC QUALITY INSPECTED 8

94-23927



94 7 27 100

**FIRST PRINCIPLES INVESTIGATION OF THE  
Ir-Zr-Nb TERNARY SYSTEM**

by  
**GREGORY A. MILLER, B.S.**

**THESIS**

**Presented to the Faculty of the Graduate School of  
The University of Texas at Austin  
in Partial Fulfillment  
of the Requirements  
for the Degree of  
MASTER OF SCIENCE IN ENGINEERING**

**THE UNIVERSITY OF TEXAS AT AUSTIN**

**May 1994**

Accession For	
NTIS CRA&I	<input checked="checked" type="checkbox"/>
DTIC TAB	<input type="checkbox"/>
Unannounced	<input type="checkbox"/>
Justification .....	
By .....	
Distribution /	
Availability Codes	
Dist	Avail and/or Special
A-1	

## ACKNOWLEDGMENTS

I would like to express my appreciation to Dr. Sanchez and Pablo Craievich for all their enlightening discussions and to Dr. Sanchez for his support and guidance throughout this project. I would also like to thank my family, mom, dad and Mike, for their continuing support.

April 20, 1994

**ABSTRACT**

**FIRST PRINCIPLES INVESTIGATION OF THE**

**Ir-Zr-Nb TERNARY SYSTEM**

by

Gregory Allen Miller

Supervising Professor: Dr. Juan M. Sanchez

Alloy design could benefit greatly from a systematic approach that combines current empirical practices with the predictive capabilities of computer modeling such as first principles based methods. At this point in time, realization of such an aid to alloy design requires the investigation of alloying systems based on first principles approaches to determine ultimate limitations and gauge the merits of this type of predictive method. The following study begins an investigation of the Ir-Zr-Nb ternary system based on combining first principles total energy calculations with a statistical mechanics description of solids.

The Ir-Zr-Nb ternary system was initially chosen for the two highly ordered binary systems, Ir-Zr and Ir-Nb, and, more specifically, for coordinating with experimental work on the  $\text{Ir}_3\text{Zr}_{1-x}\text{Nb}_x$  system. The two main contributions of this study include compiling a database of first principles data for fcc- and bcc-based compounds for the Ir-Zr-Nb ternary system, and calculating the Ir-Zr-Nb fcc metastable ternary phase diagram.

First principles total energy calculations were performed using the linearized muffin-tin orbital (LMTO) method in the atomic sphere approximation (ASA). The database includes LMTO-ASA total energies and subsequent curve fitting parameters for fifteen fcc-based compounds and twenty-one bcc-based compounds. Results of calculations compared well with all experimental data found. Highlights include: i) correctly predicting the stability of Ir as fcc, Nb as bcc, IrZr as B2, IrNb as  $L1_0$ ,  $Ir_3Zr$  as  $L1_2$ , and  $Ir_3Nb$  as  $L1_2$ , ii) a trend of increasing bulk moduli with content Nb for Nb-Zr compounds, and iii) calculation of the formation energy of IrZr-B2 to within 4 %. Formation energies for fcc-based compounds were then combined with a statistical mechanics model using the Cluster Variation Method (CVM) in the tetrahedron approximation for configurational entropies, and the cluster expansion of Sanchez, Ducastelle, and Gratias for calculating free energies for the Ir-Zr-Nb fcc metastable ternary phase diagram.

Results of ternary calculations include a single phase  $Ir_3Zr$  ( $L1_2$ ) and  $Ir_3Nb$  ( $L1_2$ ) region, the appearance of both the IrZr ( $L1_0$ ) and IrNb ( $L1_0$ ) ordered phases, and two miscibility gaps between two  $L1_2$  phases and between two disordered phases. The main conclusion of the phase diagram calculations is that serious improvement will require combining the effects of bcc- and, possibly, hcp-based compounds with those of the fcc-based compounds.

## TABLE OF CONTENTS

Introduction	1
First Principles Calculations	3
Free Energy Model	8
Results	13
Database Results	18
Metastable fcc Ternary Phase Diagram	26
Conclusions and Recommendations	32
Appendix: Morse Potential Parameters	34
Bibliography	36
Vita	38

## LIST OF TABLES

Table 1. Crystal structures used for LMTO-ASA calculations with Strukturbericht nomenclature.	15
Table 2. Crystal structures used for LMTO-ASA calculations with Strukturbericht nomenclature.	16
Table 3. Calculated and experimental ground state properties for pure elements and binary compounds in the Ir-Zr-Nb system.	19
Table 4. Calculated ground state properties for ternary compounds in the Ir-Zr-Nb system.	24

## LIST OF FIGURES

Figure 1. Tetrahedron cluster for the fcc and bcc crystal structures.	11
Figure 2. Formation energies for intermetallic compounds in the Ir-Nb system.	20
Figure 3. Formation energies for intermetallic compounds in the Ir-Zr system.	21
Figure 4. Formation energies for intermetallic compounds in the Nb-Zr system.	22
Figure 5. Bulk moduli for intermetallic compounds in the Nb-Zr system.	22
Figure 6. Formation energies for intermetallic compounds in the Ir-Zr-Nb system.	23
Figure 7. Isotherm for the Ir-Zr-Nb system at 1200 K.	27
Figure 8. Isotherm for the Ir-Zr-Nb system at 1500 K.	29
Figure 9. Isotherm for the Ir-Zr-Nb system at 1700 K.	30
Figure 10. Isotherm for the Ir-Zr-Nb system at 1900 K.	31



## Introduction

Intermetallic alloy design is still largely conducted by trial and error and alloy specific methods. This involves the addition of various alloying elements to tailor a material to desired properties. The need exists for an intelligent and interactive alloy design methodology to better guide time intensive experimental methods on new intermetallic systems. An approach that combines predictive methods such as first principles calculations with experimental work would allow for the development of such a design methodology. Currently, first principles methods have been developed to the point of allowing the calculation of many properties of simple materials based solely on input of atomic numbers, atomic masses and atomic positions in a given crystalline structure. When combined with an accurate statistical mechanics theory, this allows the finite temperature calculation of equilibrium and metastable phases. The computational approach to the determination of the thermodynamic properties of materials is especially useful for cases where little or no experimental work exists, such as multicomponent intermetallic systems. Here I present the results of a preliminary investigation into the Ir-Zr-Nb system.

The Ir-Zr-Nb system was chosen with consideration for its high temperature stability. The future of high temperature superalloys requires finding suitably ductile intermetallic systems with melting temperatures higher than the current generation of nickel base superalloys ( $T_{\text{melt}} \sim 1,385^\circ\text{C}$ ). The Ir-Zr-Nb system contains several  $L1_2$  phases with melting temperatures in excess of  $2,200^\circ\text{C}$ . The two  $L1_2$  compounds,  $\text{Ir}_3\text{Nb}$  and  $\text{Ir}_3\text{Zr}$ , belong to a class known as Engel-Brewer intermetallics, which are very stable transition metal compounds with high melting points. Intermetallics with the  $L1_2$  structure offer the possibility of enhanced ductility due to the large number of possible slip systems compared to more complex structures.

Therefore, we have begun a systematic electronic structure and thermodynamic study of stable and metastable compounds for the Ir-Zr-Nb ternary system. The goals of this study include documenting a database of physical properties obtained using first principles electronic structure calculations for compounds in the Ir-Zr-Nb ternary system, and partial determination of the Ir-Zr-Nb ternary phase diagram. Thus, first principles electronic structure calculations have been carried out on thirty compounds and six pure elements based on fcc and bcc crystal structures. The results of these calculations have been analyzed for trends and compared with experimental data to confirm their overall accuracy. The total energies as calculated by first principles methods were then incorporated into a free energy model to begin characterization of the Ir-Zr-Nb ternary phase diagram by calculation of the fcc metastable phase diagram.

The next two sections present the theoretical background used to obtain first principles ground state properties and the free energy model used to investigate high temperature stability. This is followed by a presentation of results, subsequent conclusions, and recommendations for future work.

## First Principles Calculations

In the last 30 years, first principles methods have progressed to become a reliable and accepted way of obtaining total energies of simple metals and ordered intermetallic compounds. Common to several first principles techniques currently in use are the Born-Oppenheimer approximation of separating the degrees of freedom of nuclei and electrons, and the use of the local density approximation which reduces the many body problem to the single-electron approximation. Various approaches include using large numbers of plane waves (e.g. augmented plane wave method), using a minimum set of basis functions while assuming a shape for the potential (e.g. linearized muffin-tin orbital method) and various combinations of these two. These techniques have been successful in a wide range of applications regarding thermal and cohesive properties of elemental transition metals [1], superconductivity [2], structural stability of elements and compounds [3], effects of ternary additions [4], elucidating empirical theories [5] and modeling diatomic molecules [6]. Particularly important to the success of first principles calculations is the acceptance of the local density approximation, LDA, [7] of the density functional theory [8] of Hohenberg and Kohn, as an accurate description of both small and extended systems. For more information on approximations used prior to the LDA and some LDA criticisms see reference [9].

Density functional theory states that the total energy of a system can be expressed as a functional of the total charge density and, furthermore, that this energy functional is minimized at the correct ground state charge density. In one formulation, the energy functional can be cast in a form which separates the effects of the true

interacting system into components modeling the non-interacting electrons and the effects of the interacting system. This energy functional includes three contributions, which are all dependent on the charge density,  $n(r)$ :

$$E(n) = T(n) + U(n) + E_{xc}(n) \quad (1)$$

The first two terms in equation (1) contain energies based on a system of non-interacting electrons while the last term accounts for effects due to exchange and correlation. The first two terms are, respectively, the kinetic energy,  $T(n)$ , of a system of non-interacting particles of charge density  $n(r)$ , and the potential energy,  $U(n)$ , due to contributions from the interaction of  $n(r)$  with itself, of  $n(r)$  with the nuclei, and Coulombic interactions between nuclei. The last term,  $E_{xc}(n)$ , includes the many-body effects of exchange and correlation.

Hohenberg and Kohn have shown that the correct electron (or charge) density can be obtained by solving a one-electron Schrödinger-like equation:

$$(-\nabla^2 + V)\psi_j = E_j\psi_j \quad (2)$$

obtained by minimization of the previously mentioned energy functional subject to the constraint of a constant number of electrons. The effective potential,  $V$ :

$$V = U_c + V_{xc} \quad (3)$$

is comprised of  $U_c$ , the Coulomb potential, and  $V_{xc}$ , the potential due to exchange

and correlation effects. A summation over the one-electron wave functions of all occupied states gives the total charge density:

$$n(r) = \sum_i |\psi_i|^2 \quad (4)$$

This result can then be used to obtain the Coulomb contribution,  $U_c$ , to the effective potential through solution of Poisson's equation:

$$\nabla^2 U_c = -8\pi n(r) \quad (5)$$

Determination of the correct ground state requires the self-consistent solution of equations (2) through (5). However, the correct form for the contribution to the effective field due to exchange-correlation must be determined. It is at this point that the approximation of importance to first principles calculations is introduced.

The local density approximation involves writing the exchange-correlation energy,  $E_{xc}(n)$ , as:

$$E_{xc}(n) = \int n(r) \epsilon_{xc}(n(r)) dr \quad (6)$$

where  $\epsilon_{xc}(n(r))$  is the exchange and correlation energy per electron of a uniform electron gas of charge density  $n(r)$  [7]. The exchange-correlation energy can now be connected with the Schrödinger-like equation via the relation:

$$V_{xc} = d(n\epsilon_{xc}(n)) / dn \quad (7)$$

The LDA is exact only in the limit of a constant electronic density and, although most real systems such as atoms, molecules or solids show strong variations within a local Fermi wavelength, the LDA has proven more accurate than would be expected.

For our total energy calculations we used the linearized muffin-tin orbital method (LMTO) in the atomic sphere approximation (ASA). For a complete and in depth derivation of the LMTO-ASA method including program code, see Skriver's publication [10]. The LMTO method applies the variational principle to Schrödinger's equation using energy independent basis functions such that the resulting secular equations are linear in energy. Thus the problem is reduced to solving an eigenvalue problem of  $9 \times 9$  (s, p and d states) per atom at each point in reciprocal space.

The atomic sphere approximation (ASA) involves replacing the atomic polyhedron of Wigner and Seitz with a sphere at each atomic position. This atomic polyhedron is created by perpendicular planes bisecting *interatomic distances*. For pure elements, the atomic volume is equal to a sphere of Wigner-Seitz radius. For compounds, the average of the various atomic volumes is equal to a sphere for which the radius is then the effective Wigner-Seitz radius. With regard to calculations of total energies, use of the ASA involves choosing the number of radial divisions which is the only variable for spherical geometries.

For analysis of binding curves we used the Morse potential [1]. The Morse potential serves merely as a convenient function for fitting binding curves although it merits no phenomenological significance. The fitting of this function allows for

estimates for the bulk modulus, Debye temperature, and Grüneisen constant. The total energy,  $E$ , is written in terms of the Wigner-Seitz radius,  $r$ , as:

$$E(r) = A + Ce^{-2\lambda(r-r_0)} - 2Ce^{-\lambda(r-r_0)} \quad (8)$$

where  $A$ ,  $C$ ,  $\lambda$ , and  $r_0$  are four fitting parameters. The parameters represent the cohesive energy,  $C$ , the total energy,  $A-C$ , the equilibrium Wigner-Seitz radius,  $r_0$ , and a fitting variable,  $\lambda$ . In terms of the above parameters we have for the bulk modulus:

$$B(r_0) = \frac{C\lambda^2}{6\pi r_0} \quad (9)$$

where  $r_0$  is in a.u.,  $\lambda$  is in a.u.<sup>-1</sup>,  $C$  is in Ry/atom, and  $B$  is in Bar. The Debye temperature and Grüneisen constant can also be expressed in terms of the fitting parameters:

$$\gamma = \frac{r_0\lambda}{2} \quad (10)$$

$$\theta = 41.63 \left( \frac{r_0 B}{M} \right)^{1/2} \quad (11)$$

where  $\gamma$  is the Grüneisen constant,  $\theta$  is the Debye temperature expressed in Kelvin, and  $M$  is the atomic weight.

## Free Energy Model

Calculation of phase stability of disordered alloys at finite temperatures has previously been carried out by using either empirical methods or phenomenological models. An example of the empirical approach is the method introduced by Kaufman and Nesor [11], widely used, which involves fitting simple functions to available thermochemical data, including phase diagram information. In some cases these functions can then be extrapolated into unexplored regions of phase diagrams. While these empirical methods have proven useful for prediction of phase stability, they are limited to systems for which experimental data is available. Therefore, their use in the development of new systems is questionable.

A more fundamental approach is based on the description of the statistical thermodynamics of an alloy in terms of clusters of lattice sites with effective cluster interaction energies provided by either phenomenological models or first principles calculations. The accuracy of these models is usually improved by increasing the cluster size from point, to pair to larger size atomic interactions. However, complexity of the formalism and computation time increase as well. Some lower level approximations include the Bragg-Williams or point approximation, the Bethe or pair approximation, and the quasi-chemical approach of Guggenheim. A more generalized description of the configurational thermodynamics of alloys was provided in 1951 by the Cluster Variation Method (CVM) of Kikuchi [12], which involves a hierarchy of cluster sizes that allows for any level of approximation. Originally developed to improve upon the mean-field and quasichemical combinatorial methods of treating simple models of magnetism, the CVM has since undergone several developments including the study of prototype phase diagrams involving first order transitions [13] and the use of the method for studying real binary systems [14]. The current use of the



CVM is based on a general formalism for the description of configurational cluster functions in multicomponent systems as developed by Sanchez, Ducastelle and Gratias [15].

The formalism of Sanchez, Ducastelle, and Gratias involves a cluster expansion. This expansion is based on a one to one correspondence between the set of clusters of lattice points in a crystal and orthogonal functions which describe the configuration of a system in terms of spin (or occupation) numbers for each site. An N-dimensional vector of the occupation numbers will completely specify any configuration of a system. The practical result of this formalism is that any function of configuration can be derived in terms of a sum over all clusters in the crystal up to a specified maximum cluster size. This maximum cluster size allows control of desired level of approximation. The cluster expansion may then be combined with the energies of a set of ordered compounds, for which the orthogonal basis functions can be determined, in order to obtain effective cluster interactions. These interactions, in turn, can be used to describe the disordered system.

Based on the success of this cluster description of the energy of alloys, Connolly and Williams [16] combined first principles calculations with the cluster expansion in order to determine the energy of formation of disordered transition metal alloys. Subsequently, other investigations combining first principles calculations and the CVM have shown this method to provide a reliable description of disordered systems from ordered systems [17, 18, 19], including the successful application to the modeling of ternary systems [20, 21]. Combining the CVM with first principles calculations was a natural choice for our preliminary investigation of the Ir-Zr-Nb ternary phase diagram.

The free energy model used accounts for contributions due to formation energies and configurational effects. The total free energy per phase,  $F^\alpha$ , is:

$$F^\alpha = \Delta H_f - TS_{\text{conf}} \quad (12)$$

where  $\Delta H_f$  is the energy of formation,  $T$  is the temperature, and  $S_{\text{conf}}$  is the configurational entropy. Neglected in this model are structural energies and vibrational effects. For the current use of the free energy model, calculations are performed only for compounds based on the fcc crystal structure. Therefore, structural energies will contribute equally to phase stability of all compounds and can be neglected. Although vibrational effects will contribute considerably to the total free energy of a compound, the calculation of phase diagrams requires energy differences for which these effects should be small.

Formation energies involve a summation of cluster energies over their respective cluster probabilities:

$$\Delta H_f = \sum_{ijkl} \epsilon_{ijkl} Z_{ijkl} \quad (13)$$

where  $Z_{ijkl}$  is the probability of a tetrahedron cluster of configuration  $ijkl$ , and  $\epsilon_{ijkl}$ :

$$\epsilon_{ijkl} = \epsilon'_{ijkl} - C_a \epsilon'_{aaaa} - C_b \epsilon'_{bbbb} - C_c \epsilon'_{cccc} \quad (14)$$

is the formation energy of cluster of configuration  $ijkl$  for which  $\epsilon'$  are the total energies as obtained from LMTO-ASA calculations. By carefully choosing ordered

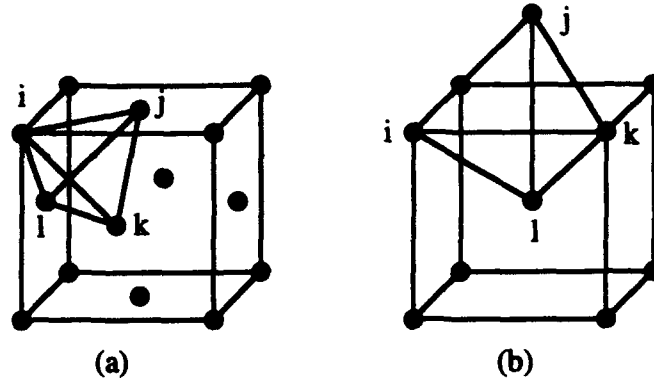


**Figure 1.** Tetrahedron clusters for the (a), fcc, and (b), bcc, crystal structures. Temperature dependence of the formation energy is implicit in the cluster probabilities.

intermetallic systems comprised of a given tetrahedron cluster (see Figure 1), the resulting total energies will be those of the tetrahedron clusters.

Configurational entropy is accounted for by using the cluster variation method in the tetrahedron approximation. Using tetrahedra as the largest cluster includes triangle, pair and point contributions in the approximation. This level of cluster approximation accounts for first nearest neighbors in fcc-based phases and first and second nearest neighbors in bcc-based phases. Increasing the accuracy of the CVM requires using larger clusters. However, this also significantly increases the complexity of the formalism. The configurational entropy per lattice point is:

$$S_{\text{conf}}^{\text{fcc}} = -k_B \left( 2 \sum_{ijkl} Z_{ijkl} \ln Z_{ijkl} - 6 \sum_{ij} Y_{ij} \ln Y_{ij} + 5 \sum_i X_i \ln X_i \right) \quad (15)$$

where  $k_B$  is Boltzmann's constant. The variables in the equation (15) are the tetrahedron cluster probabilities,  $Z_{ijkl}$ , and the sub-cluster probabilities for point

clusters ( $X_i$ ), and pairs ( $Y_{ij}$ ). The following equations show the relationship between each sub-cluster and the tetrahedron probabilities.

$$\begin{aligned} X_i &= \sum_{jkl} Z_{ijkl} \\ Y_{ij} &= \sum_{kl} Z_{ijkl} \end{aligned} \tag{16}$$

Using the thermodynamic definition of the chemical potential for a single component, a grand potential can be derived. In the grand potential per phase,  $G^\alpha$ :

$$G^\alpha = F^\alpha - \sum_i X_i \mu_i^\alpha \tag{17}$$

$X_i$  is the composition of pure element  $i$ ,  $\mu_i^\alpha$  is the chemical potential of element  $i$  in phase  $\alpha$ , and  $F^\alpha$  is the free energy per phase from equation (10). The arithmetic mean of the chemical potentials is set at zero for the reference state.

Determination of the equilibrium atomic arrangement at a given temperature requires differentiation of the grand potential with respect to  $Z_{ijkl}$ , the tetrahedron cluster probabilities, while fixing the chemical potential. This differentiation results in a set of non-linear algebraic equations from which the tetrahedron cluster probabilities can be solved for iteratively using the Natural Iteration Method [22].

The following sections contain a discussion of our results and ends with conclusions and recommendations for future work.

## Results

The investigation of the Ir-Zr-Nb ternary system is based on using the linearized muffin-tin orbital method in the atomic sphere approximation (LMTO-ASA) for the calculation of first principles total energies, and using a cluster expansion to calculate free energies and the ternary phase diagram. LMTO-ASA total energy calculations have been performed for the pure elements and selected binary and ternary compounds based on the bcc and fcc crystal structures. For each compound and/or pure element, the calculation gives cohesive energies, formation energies, total energies, equilibrium volumes, lattice constants, bulk moduli, Debye temperatures, and Grüneisen constants for which the only input is the atomic numbers. Our calculations also reveal the relative stability of different structures and allow us to observe trends in alloying. The results of the LMTO-ASA total energy calculations for fcc-based compounds have been further used to calculate the fcc metastable ternary phase diagram for the Ir-Zr-Nb system. The following sections contain discussions on the level of approximations used in calculations, a description of all structures investigated, and a presentation of the results of calculations and analysis of these results. Presentation of calculated results is further divided into database related information followed by calculated isothermal sections of the Ir-Zr-Nb ternary phase diagram.

### Approximations

The LMTO-ASA calculations used no spin orbit coupling, 900 points in the atomic sphere approximation (described in first principles section), and an average of 800 to 1000 k-points in the irreducible wedge of the Brillouin zone in reciprocal space. By increasing the number of points used to describe the atomic sphere approximation, I found that the total energies of pure elements and several compounds leveled off for a number of points in excess of 800. Spin orbit (SPO) effects have clearly been shown

to be important for transition metals with atomic number greater than fifty. Therefore, there was concern over the neglect of SPO effects for Iridium compounds. We note that calculations comparing pure elements show that including SPO effects increases the total energies by .293, .016 and .026 (Ryd/atom) for fcc Ir, Zr and Nb, respectively. Also, three compounds,  $\text{Ir}_3\text{Nb}$  ( $\text{D0}_3$ ),  $\text{Ir}_2\text{ZrNb}$  ( $\text{D0}_3$ -like), and  $\text{Ir}_3\text{Zr}$  ( $\text{D0}_3$ ), were tested, with and without SPO effects, for which formation energies were compared (see Table 1 for structures). The formation energies for calculations including SPO effects increased by 3.48, 5.44, and .666 (mRyd/atom), for  $\text{Ir}_3\text{Nb}$ ,  $\text{Ir}_2\text{ZrNb}$ , and  $\text{Ir}_3\text{Zr}$ , respectively. Although calculations including SPO effects had less negative total energies, trends in alloying properties such as relative stability and bulk moduli remained constant.

### Crystal Structures

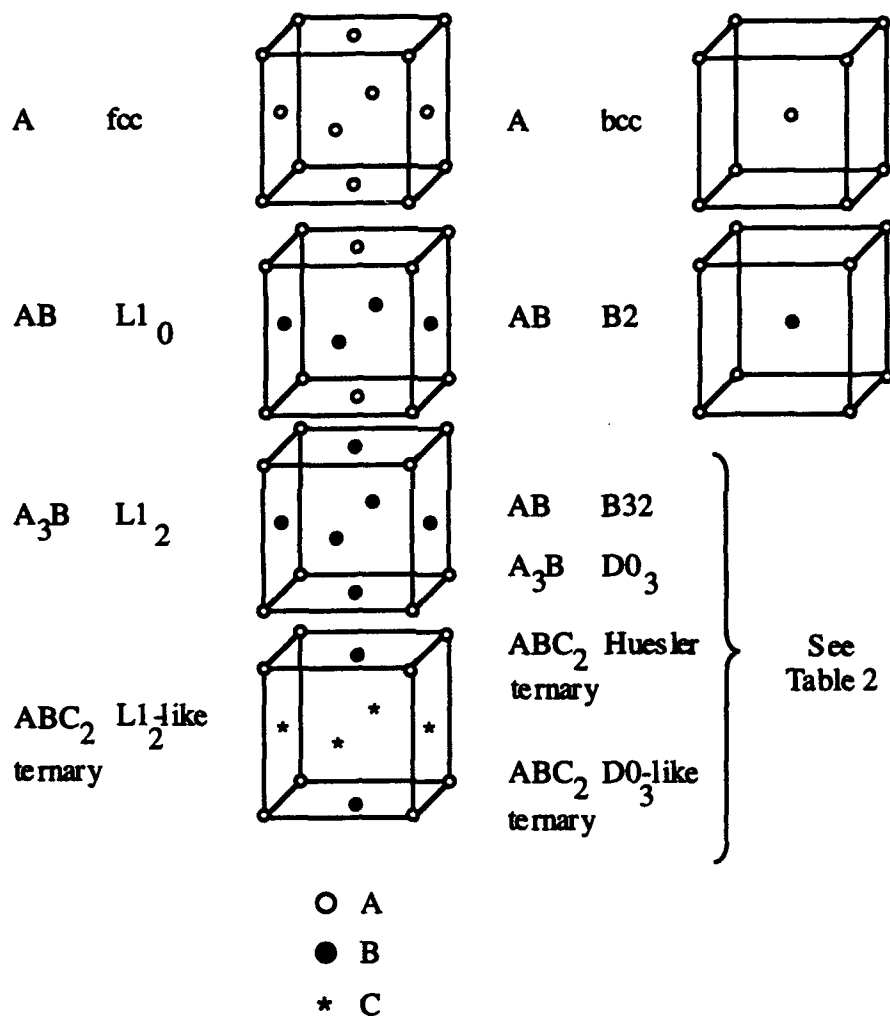
Crystal structures were chosen to accommodate for all possible configurations of the tetrahedron clusters described in the free energy model section (see Figure 1). Of the thirty-six structures evaluated, fifteen were based on the fcc crystal structure while twenty-one were based on the bcc crystal structure. Table 1 below shows some of the simpler structures, according to Strukturbericht nomenclature, used for the LMTO-ASA calculations, while Table 2 contains the more complex bcc-based compounds, including two binary compounds and both ternary compounds.

Six of the thirty-six structures correspond to the three elements in both fcc and bcc crystal structures. For binary compounds, fcc-based compounds include the  $\text{L1}_2$  ( $\text{A}_3\text{B}$ ) and the  $\text{L1}_0$  ( $\text{AB}$ ) structures, while bcc-based compounds include  $\text{D0}_3$  ( $\text{A}_3\text{B}$ ) and  $\text{B2}$  ( $\text{AB}$ ). Ternary compounds,  $\text{ABC}_2$ , include the fcc-based compound ( $\text{L1}_2$ -like) and the two bcc-based compounds (Huesler alloy and  $\text{D0}_3$ -like). The two bcc-based ternary compounds are distinguished such that the Huesler alloy is comprised of bcc

tetrahedra with atoms A and B as first nearest neighbors and the  $DO_3$ -like compound is comprised of bcc tetrahedra with atoms A and B as second nearest neighbors.

**Table 1**

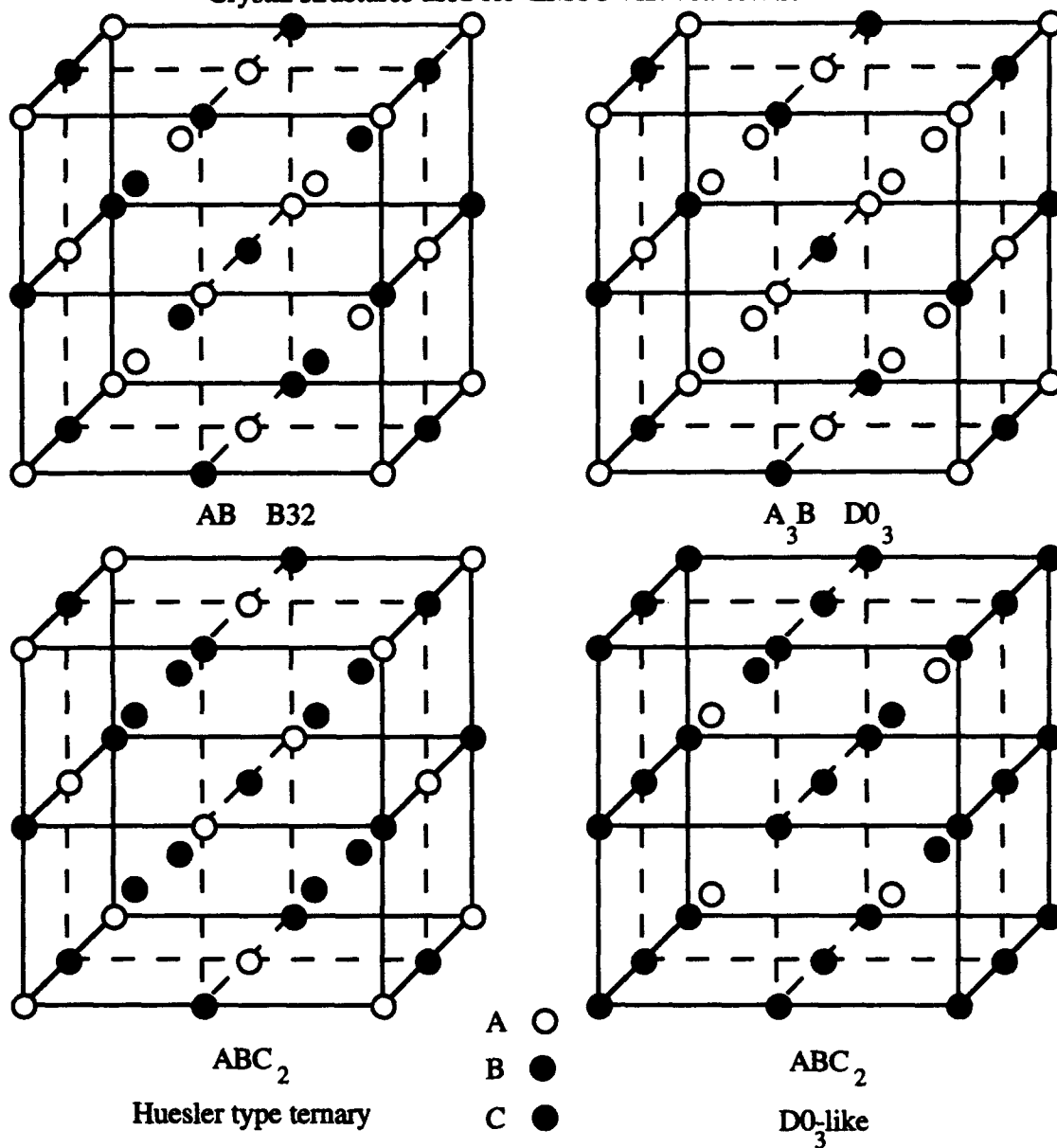
Crystal structures used for LMTO-ASA calculations  
with Strukturbericht nomenclature.



By using these chosen structures, one can see that all four combinations of atoms for the bcc and fcc tetrahedra are tested for at least one bcc- and fcc-based

**Table 2**

Crystal structures used for LMTO-ASA calculations.



structure, while the AB and  $ABC_2$  compounds are each tested for an additional bcc-based structure. The various ordered compounds used for LMTO-ASA calculations were chosen to accommodate for all possible configurations of fcc and bcc tetrahedron



clusters. From the resulting LMTO-ASA total energies, effective interactions can be determined for all possible configurations of Ir, Zr and Nb on the fcc and bcc tetrahedra. The bcc compounds require extra structures, relative to the fcc compounds, because the bcc tetrahedron includes first and second nearest neighbors allowing for more configurations.

## Database Results

In comparing our results with experimental data, it serves best to examine phase stability first. Those compounds that represent stable alloys can be further compared to experimental data while metastable compounds can only be correlated to trends. The results are separated by first discussing pure elements, then each binary system, followed by the ternary compounds, and finally, any overall trends. As discussed in the first principles section, all calculated values are based on fitting binding curves with the Morse potential. The values for the Morse potential parameters for all compounds are contained in the Appendix. The fit provided by the Morse potential was compared with the original calculated first principles total energies and resulted in excellent agreement.

### Pure Ir, Zr, and Nb

Beginning with the pure elements, calculations correctly predict the stability of Iridium as fcc and Niobium as bcc. Zirconium, however, is stable as hcp while our calculations of bcc and fcc structures only showed Zirconium to be more stable as bcc. Table 3 contains the calculated lattice parameters, bulk moduli, Debye temperatures, and Grüneisen constants for pure elements and binary compounds including available experimental data. As seen in Table 3, Niobium (bcc) agrees well with the experimental values for bulk modulus, Debye temperature and Grüneisen constant.

Table 3

Calculated and Experimental Ground State Properties for Pure Elements and for Binary Compounds in the Ir-Zr-Nb System.

Crystal Structure	Lattice Con.(Ang)		Bulk Mod (Mbar)		Debye Temp. (K)		Grüneisen	
	Calc.	Exp.	Calc.	Exp.	Calc.	Exp.	Calc.	Exp.
Ir (fcc)	3.926	3.839*	3.689		310	420 ⊕	1.89	
Ir (bcc)	3.152		3.503		304		1.93	
Zr (fcc)	4.625		1.139		272		1.42	
Zr (bcc)	3.659		1.131		270		1.41	
Nb (fcc)	4.309		1.926		338		1.64	
Nb (bcc)	3.393	3.3002*	2.041	1.702 ⊕	347	275 ⊕	1.64	1.58 ⊕
Ir <sub>3</sub> Nb (L1 <sub>2</sub> )	3.990	3.886*	3.520		328		1.86	
Ir <sub>3</sub> Nb (D0 <sub>3</sub> )	3.203		3.122		310		1.83	
IrNb (L1 <sub>0</sub> ) **	4.08	4.027, 3.863*	2.981		330		1.79	
IrNb (B2)	3.269		2.766		320		1.77	
IrNb (B32)	3.248		2.782		320		1.75	
IrNb <sub>3</sub> (L1 <sub>2</sub> )	4.189		2.414		332		1.71	
IrNb <sub>3</sub> (D0 <sub>3</sub> )	3.313		2.493		336		1.71	
Ir <sub>3</sub> Zr (L1 <sub>2</sub> )	4.057	3.943*	3.053		308		1.77	
Ir <sub>3</sub> Zr (D0 <sub>3</sub> )	3.257		2.743		294		1.75	
IrZr (L1 <sub>0</sub> )	4.222		2.318		297		1.66	
IrZr (B2)	3.370	3.318*	2.267		294		1.65	
IrZr (B32)	3.346		2.167		287		1.61	
IrZr <sub>3</sub> (L1 <sub>2</sub> )	4.414		1.639		282		1.54	
IrZr <sub>3</sub> (D0 <sub>3</sub> )	3.478		1.677		284		1.53	
NbZr <sub>3</sub> (L1 <sub>2</sub> )	4.539		1.311		288		1.48	
NbZr <sub>3</sub> (D0 <sub>3</sub> )	3.587		1.319		289		1.47	
NbZr (L1 <sub>0</sub> )	4.460		1.498		305		1.54	
NbZr (B2)	3.523		1.512		305		1.52	
NbZr (B32)	3.518		1.536		308		1.53	
Nb <sub>3</sub> Zr (L1 <sub>2</sub> )	4.383		1.722		323		1.60	
Nb <sub>3</sub> Zr (D0 <sub>3</sub> )	3.455		1.763		326		1.58	

\* Pearson's Handbook [23]

\*\* The IrNb-L1<sub>0</sub> experimental values reflect the tetragonal nature of the L1<sub>0</sub> type structure, while our calculations assumed cubic L1<sub>0</sub>.

⊕ American Inst. of Phys. Handbook [24]

### Ir-Nb Binary System

The relative stability of the components in the Ir-Nb binary system, as gauged by the formation energies relative to the most stable pure elements, fcc Ir, and bcc Zr and Nb, can be seen in Figure 2 below. Of the three compounds tested,  $\text{Ir}_3\text{Nb}$ , IrNb and Nb, can be seen in Figure 2 below. Of the three compounds tested,  $\text{Ir}_3\text{Nb}$ , IrNb

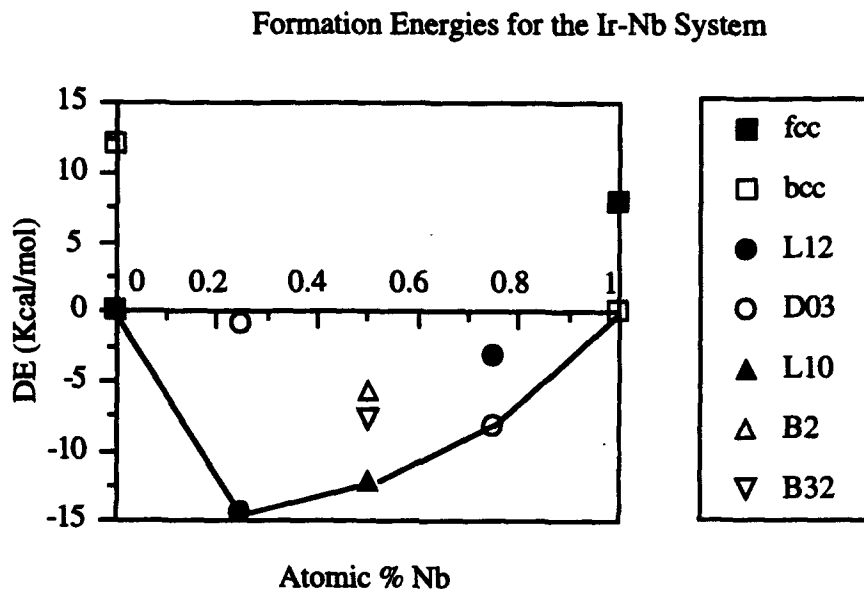


**Figure 2.** Energies of formation for intermetallic compounds in the Ir-Nb system relative to fcc Ir, and bcc Zr and Nb.

and,  $\text{IrNb}_3$  are more stable as  $\text{L1}_2$ ,  $\text{L1}_0$  and  $\text{D0}_3$ , respectively. This correctly predicts  $\text{Ir}_3\text{Nb}$  as  $\text{L1}_2$  and IrNb as  $\text{L1}_0$ .

### Ir-Zr Binary System

In agreement with the experimental binary phase diagram for the Ir-Zr system [25], the following formation energies predict  $\text{Ir}_3\text{Zr}$  and IrZr to be  $\text{L1}_2$  and B2, respectively. Also,  $\text{IrZr}_3$  is more stable as  $\text{D0}_3$ . The standard molar enthalpy of

### Formation Energies for the Ir-Zr System

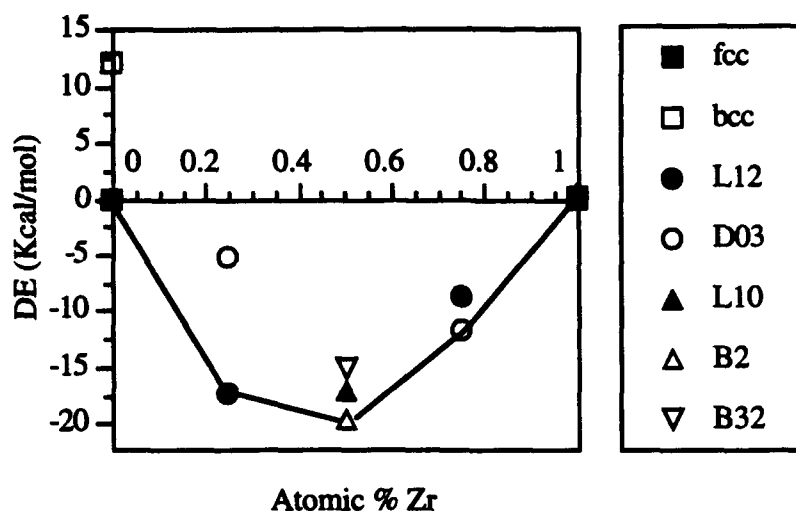


**Figure 3.** Energies of formation for intermetallic compounds in the Ir-Zr system relative to fcc Ir, and bcc Zr and Nb.

formation for IrZr-B2 was experimentally determined by Topor and Kleppa [26] to be  $-20.47 \pm .93$  Kcal/mol which agrees well with our calculated value of -19.74 Kcal/mol.

### Nb-Zr Binary System

Unlike the previous two binary systems, the Nb-Zr binary system includes a miscibility gap and, therefore, no stable intermediate phases are observed experimentally. Our calculated formation energies agree with this result. Another trend correctly

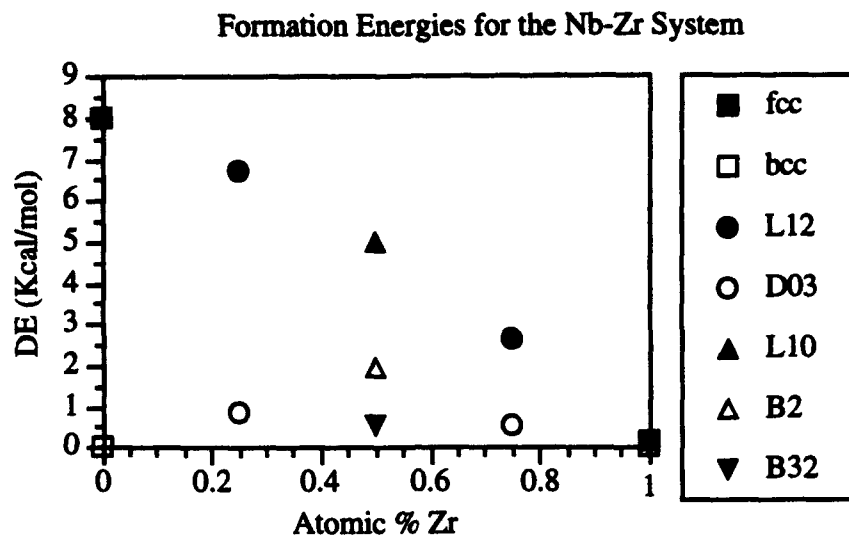


**Figure 4.** Energies of formation for intermetallic compounds in the Nb-Zr system relative to fcc Ir, and bcc Zr and Nb.

reflected by our calculations, see Figure 5, is that the stiffness of Nb-Zr alloys should increase with additional Niobium content from about 20 to 80 At% Nb [28].

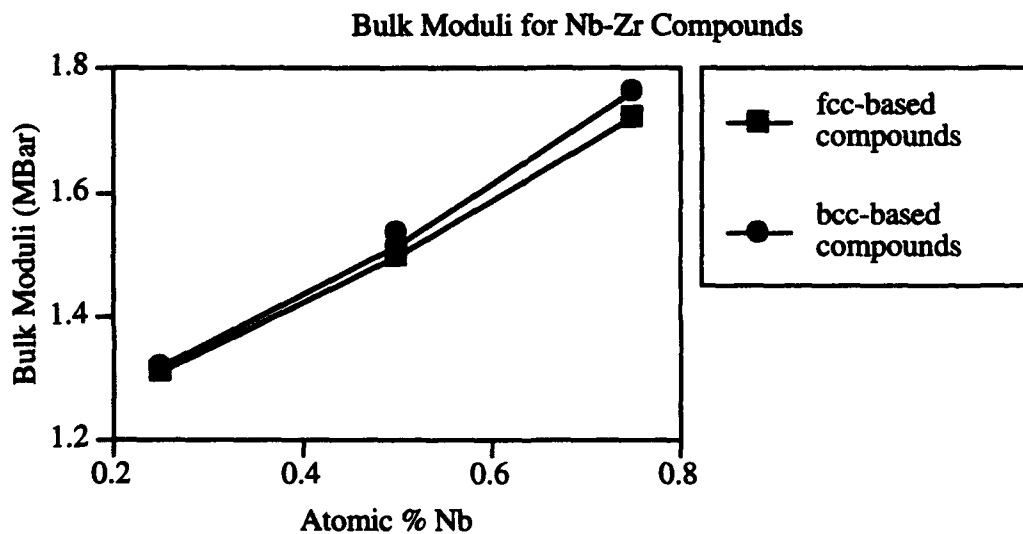


**Figure 5.** Bulk moduli, as provided by LMTO-ASA total energy calculations, versus atomic percent Niobium for the Nb-Zr system.

### Ternary Compounds

Three different ternary compounds were tested on three different structures. These crystal structures included an L1<sub>2</sub>-like structure (see table 1), a D0<sub>3</sub>-like structure, and a Huesler alloy. All ternary compounds were found to have formation energies in the range of -4 to -12 Kcal/mole with the most stable configurations being the Huesler alloy for both Ir<sub>2</sub>ZrNb and IrZr<sub>2</sub>Nb, and the D0<sub>3</sub>-like compound for IrZrNb<sub>2</sub> (see Figure 6). Table 4 contains the results of LMTO-ASA calculations for ternary compounds including lattice parameters, bulk moduli, Debye temperatures and

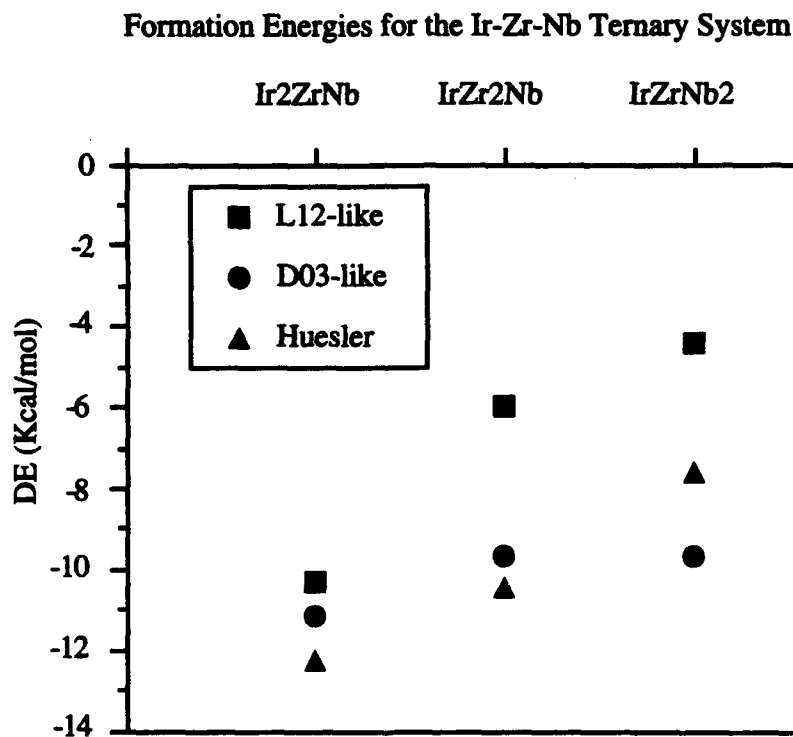


**Figure 6.** Energies of formation for intermetallic compounds in the Ir-Zr-Nb ternary system relative to fcc Ir, and bcc Zr and Nb.

Grüneisen constants. Morse potential fitting parameters are included in the Appendix. No experimental data was found concerning mechanical properties or phase stability of the tested Ir-Zr-Nb ternary compounds.

**Table 4**

Calculated Ground State Properties for Ternary Compounds in the Ir-Zr-Nb System.

Crystal Structure	Lattice Parameter (Angstrom)	Bulk Mod (Mbar)	Debye Temp. (K)	Grüneisen Constant
Ir <sub>2</sub> ZrNb (L1 <sub>2</sub> -like)	4.157	2.510	306	1.70
Ir <sub>2</sub> ZrNb (Huesler)	3.298	2.505	306	1.70
Ir <sub>2</sub> ZrNb (DO <sub>3</sub> -like))	3.320	2.513	308	1.71
IrZr <sub>2</sub> Nb (L1 <sub>2</sub> -like))	4.339	1.866	298	1.60
IrZr <sub>2</sub> Nb (Huesler)	3.417	1.910	300	1.59
IrZr <sub>2</sub> Nb (DO <sub>3</sub> -like))	3.430	1.894	299	1.58
IrZrNb <sub>2</sub> (L1 <sub>2</sub> -like))	4.265	2.102	313	1.65
IrZrNb <sub>2</sub> (Huesler)	3.365	2.182	318	1.65
IrZrNb <sub>2</sub> (DO <sub>3</sub> -like))	3.358	2.174	317	1.64

### Trends

Based on the small number of structures used, qualitative trends are few. However, through use of a linear law of mixtures, insight can be gained into non-ideal behavior. All compounds show negative deviation from linearity as applied to bulk moduli except for Ir<sub>3</sub>Nb, IrNb, Ir<sub>3</sub>Zr and IrNb<sub>3</sub>. The compounds, Ir<sub>3</sub>Nb, IrNb, and IrNb<sub>3</sub>, show stronger deviations of 7.4, 4.0, and 1.65 %, respectively, while Ir<sub>3</sub>Zr shows almost ideal behavior with a deviation of 0.1 %. The bulk moduli results for Ir<sub>3</sub>Zr and Ir<sub>3</sub>Nb agree with an experimental investigation of the Ir<sub>3</sub>Zr<sub>1-x</sub>Nb<sub>x</sub> system which showed the Young's modulus of Ir<sub>3</sub>Nb to be three times that of Ir<sub>3</sub>Zr [28]. Overall these results show that most systems lose stiffness when compounded. With regard to deviations as predicted by Vegard's law with primitive unit cell volumes, one



sees that most compounds are within 1 to 5 % of the volume predicted by the pure elements with no apparent trends.

## Metastable fcc Ternary Phase Diagram

Isothermal sections of the metastable fcc Ir-Zr-Nb ternary phase diagram were calculated to begin the eventual full characterization of this system. Calculations were performed at four different temperatures: 1200 K, 1500 K, 1700 K and 1900 K. This temperature range was sufficient to contain all important features that this simple level of free energy model encompassed. I mention again that our model involves two main contributions: formation energies, for fcc-based phases only, as supplied by LMTO-ASA calculations, and configurational entropy using the CVM in the tetrahedron approximation, which is the lowest meaningful level of the CVM allowing for first nearest neighbors. Our main goals included performing preliminary calculations for the Ir-Zr-Nb ternary phase diagram and, more specifically, investigating the  $\text{Ir}_3\text{Zr}_{1-x}\text{Nb}_x$  ternary system.

Beginning with temperatures at 1200 K and below, the results capture none of the richness expected from the two highly ordered binary systems, Ir-Nb and Ir-Zr, and fail to predict the miscibility gap for the Nb-Zr system. This of course is expected since the current model only includes contributions for fcc arrangements of atoms. The 1200 K isotherm, shown in Figure 7, reveals a miscibility gap between two disordered phases, a miscibility gap between a Nb rich and a Zr rich  $\text{L1}_2$  ordered compound, a two phase  $\text{L1}_2$  and disordered fcc phase region, and two  $\text{L1}_0$  regions for both Ir-Nb and Ir-Zr compounds. The lines running across all two phase regions in Figure 7, and similarly for all other two phase regions, represent tie lines between coexisting phases. The black regions indicate three phases coexisting.

This isotherm correctly shows the formation of the IrNb- $\text{L1}_0$  ordered compound. The two phase  $\text{L1}_2$  and fcc disordered region exists at much higher temperatures than for the experimental Ir-Zr and Ir-Nb binary phase diagrams [25].

This is due to the simple level of free energy model used which includes no provisions for calculation of the free energy of liquid phases. This isotherm does, however, show that the two binary compounds,  $\text{Ir}_3\text{Nb}$  and  $\text{Ir}_3\text{Zr}$ , form a single phase region for the

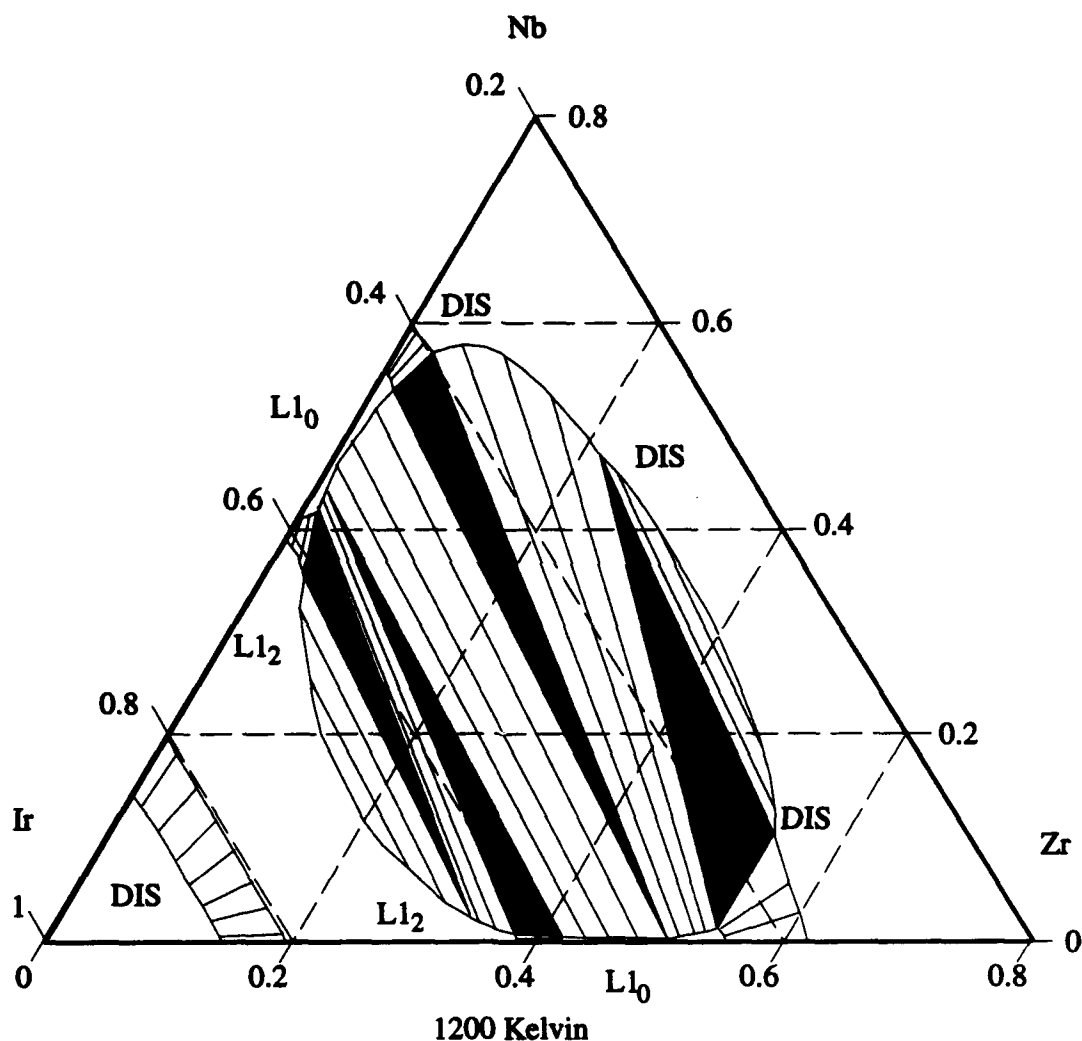


**Figure 7.** Isotherm for the Ir-Zr-Nb system at 1200 K.

$\text{Ir}_3\text{Zr}_{1-x}\text{Nb}_x$  system as expected due to the similarities between the lattice parameters of  $\text{Ir}_3\text{Nb}$  and  $\text{Ir}_3\text{Zr}$ . Lattice parameters for both compounds were within 1.6%, such that

atomic size effects might be negligible. The strength in this prediction rests on the fact that the free energy model uses energy inputs of compounds based on fcc crystal structures only. Therefore, the Iridium rich portion of the ternary phase diagram should be well represented in this approximation, at least with regard to short range ordering, while regions closer to Niobium and Zirconium should represent metastable phases and, thus, they are not observed in the equilibrium phase diagram. This single phase  $L1_2$  region points to the possibility of solid solution strengthening as a mechanism for the recently tested ternary compound,  $\text{Ir}_{.71}\text{Zr}_{.08}\text{Nb}_{.21}$ , being stronger than either  $\text{Ir}_3\text{Nb}$  or  $\text{Ir}_3\text{Zr}$  [28].

The isotherm for 1500 K contains the same features as the 1200 K isotherm with the loss of the IrNb-L1<sub>0</sub> phase and, subsequently, the loss of the L1<sub>0</sub>-L1<sub>0</sub> two phase region. Both miscibility gaps are still prevalent.

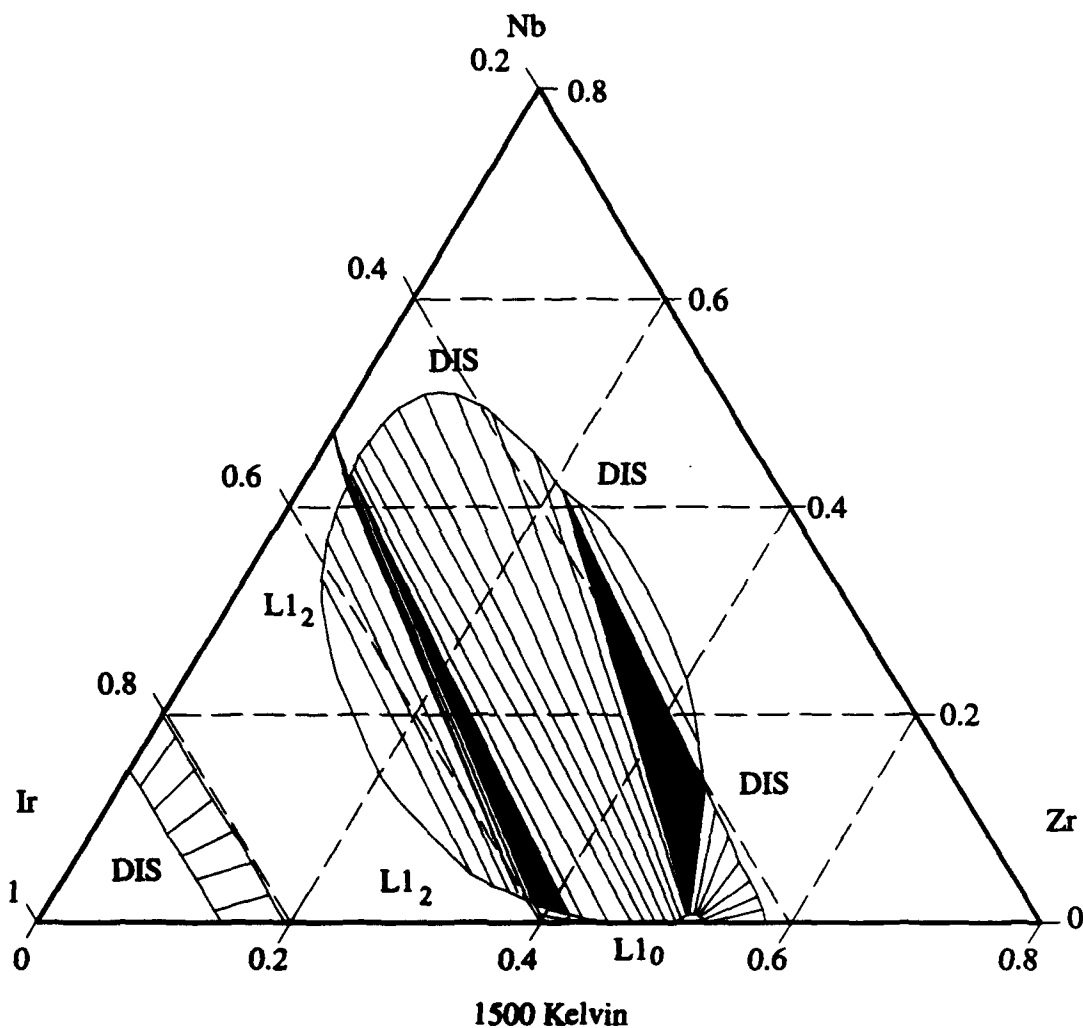


**Figure 8.** Isotherm for the Ir-Zr-Nb ternary system at 1500 K showing the loss of the IrNb-L1<sub>0</sub> phase.

The 1700 K isotherm continues the trends of the 1500 K isotherm. Also, all three phase regions have decreased in size.

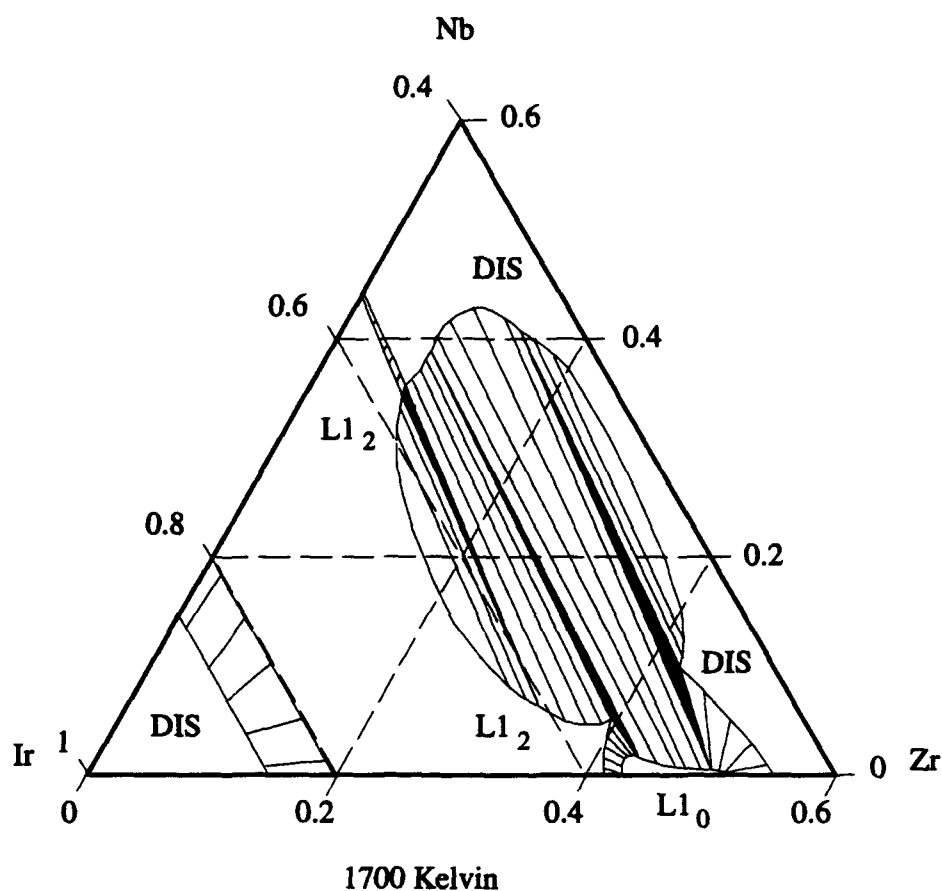


**Figure 9.** Isothermal section for the Ir-Zr-Nb ternary section at 1700 K. Black regions indicate three phases coexisting.

The remaining higher temperature isotherms contain only two phase regions: the earlier evidenced region involving the disordered fcc phase and the  $L1_2$  phase, and

a region between the  $L1_2$  phase and a disordered phase. No new features appear above 1900 K. Both  $L1_0$  phases have now vanished as well as both miscibility gaps.

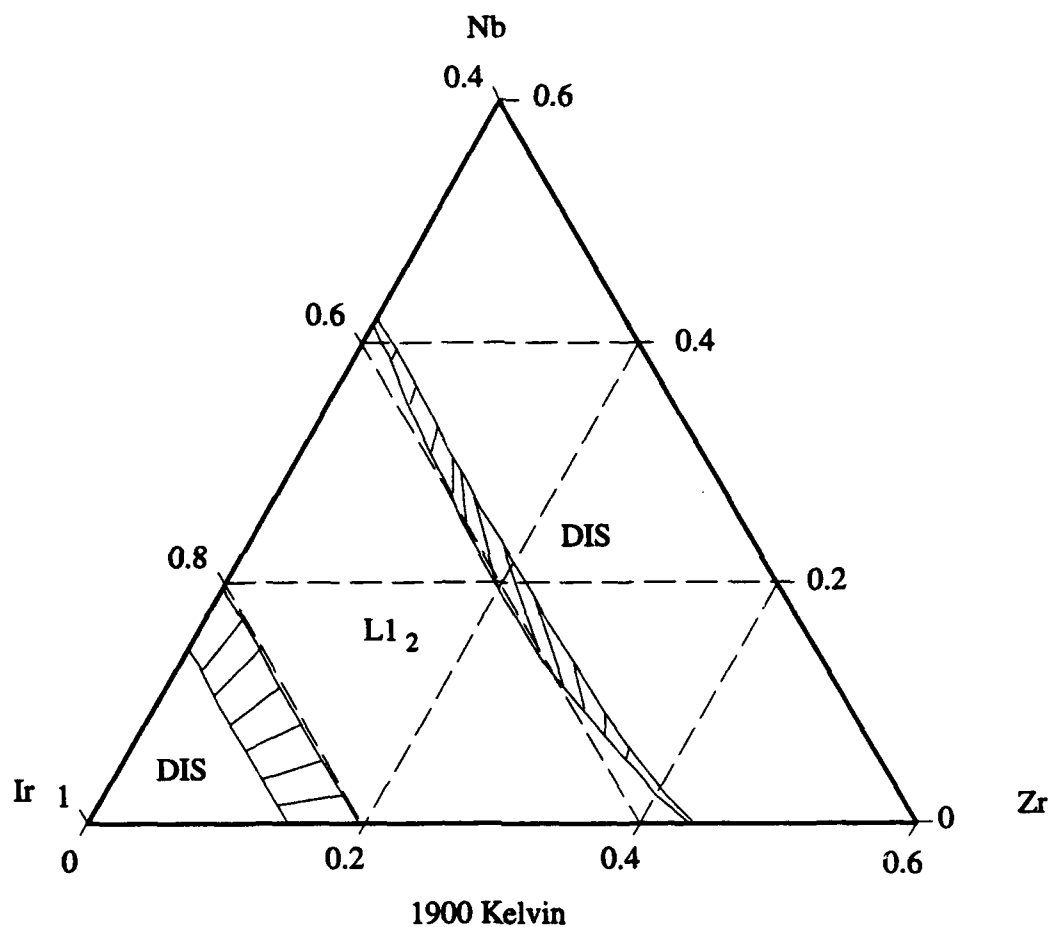


**Figure 10.** Isotherm for the Ir-Zr-Nb ternary system at 1900 K showing the remaining two phase regions.

## Conclusions and Recommendations

Calculation of binding curves and the resulting cohesive properties, Debye temperatures and Grüneisen constants was performed using the LMTO-ASA method in order to begin generating a database of physical properties for compounds in the Ir-Zr-Nb ternary system. The various levels of approximation were documented and comparisons were made with available experimental data. For the compounds that represented actual equilibrium phases, the available experimental data, including lattice parameters and formation energies, compared well with expected values. Further work with regard to LMTO-ASA calculations should be directed at possible inclusion of compounds based on the hcp crystal structure for use in the full characterization of the Ir-Zr-Nb ternary phase diagram.

We also began calculation of the Ir-Zr-Nb ternary phase diagram using input formation energies as provided by LMTO-ASA calculations, using the CVM in the tetrahedron approximation to describe configurational thermodynamics and a cluster expansion to describe the free energy. The main results showed correctly the stability of the ternary  $L1_2$  system,  $Ir_3Zr_{1-x}Nb_x$ , the  $L1_0$  IrNb ordered phase, and, most importantly, revealed that additional efforts must be employed to improve the accuracy of the simple free energy model used. It must be noted, however, that improvements in accuracy will require more than simply increasing the maximum cluster size and including vibrational effects as these changes will only shift phase boundaries. The main features, including the single phase  $L1_2$  and  $L1_0$  regions, the miscibility gap between disordered phases, and the miscibility gap between  $L1_2$  ordered phases, will remain for the fcc metastable phase diagram. Description of the equilibrium phases involves combining the free energy results of fcc-based compounds with those of bcc- and, possibly, hcp-based compounds. Therefore, additional work to be done for the



eventual full characterization of the Ir-Zr-Nb ternary phase diagram includes incorporating the effects of energies of bcc- and hcp-based compounds, modeling vibrational effects, and testing for the convergence of the effective cluster interactions to determine what range of nearest neighbor interactions must be included in the calculations.

The Ir-Zr-Nb system is undoubtedly an excellent system for exploring the connections between mechanical properties and the underlying atomistic factors that are responsible. The binary compounds,  $\text{Ir}_3\text{Nb}$  and  $\text{Ir}_3\text{Zr}$ , are similar enough to reduce many variables such as cohesive, ordering and formation energies and, therefore, provide an almost ideal system for advancing our current understanding of the mechanical behavior of intermetallic compounds.

## Appendix

The following Appendix contains all parameters used in the fitting of binding curves with the Morse potential [1]. The fitting of this function allows for estimates for the bulk modulus, Debye temperature, and Grüneisen constant. The total energy,  $E$ , is written in terms of the Wigner-Seitz radius,  $r$ , as:

$$E(r) = A + Ce^{-2\lambda(r-r_0)} - 2Ce^{-\lambda(r-r_0)}$$

where  $A$ ,  $C$ ,  $\lambda$ , and  $r_0$  are four fitting parameters. The parameters represent the cohesive energy,  $C$ , the total energy,  $A-C$ , the equilibrium Wigner-Seitz radius,  $r_0$ , and a fitting variable,  $\lambda$ .

**Table 1**  
Morse parameters for the Ir-Zr-Nb system as fit to LMTO-ASA calculations.

Crystal Structure	$r_0$ (a.u.)	$\lambda$ (a.u. <sup>-1</sup> )	C (Ryd)	A (Ryd)
Ir (fcc)	2.899892	1.307624	.801656	.382372
Ir (bcc)	2.933036	1.313567	.763108	.382372
Zr (fcc)	3.415488	.831499	.720940	.192230
Zr (bcc)	3.404107	.826975	.721381	.192230
Nb (fcc)	3.182551	1.033571	.735241	.687312
Nb (bcc)	3.157243	1.041800	.760747	.687312
Ir <sub>3</sub> Nb (L1 <sub>2</sub> )	2.946794	1.259961	.837302	.208607
Ir <sub>3</sub> Nb (D0 <sub>3</sub> )	2.980336	1.225384	.794103	.208607
IrNb (L1 <sub>0</sub> )	3.014884	1.184985	.820021	.034842
IrNb (B2)	3.041828	1.161256	.799538	.034842
IrNb (B32)	3.022169	1.155972	.806330	.034842
IrNb <sub>3</sub> (L1 <sub>2</sub> )	3.093720	1.107059	.78076	-.138923
IrNb <sub>3</sub> (D0 <sub>3</sub> )	3.082230	1.11572	.797007	-.138923
Ir <sub>3</sub> Zr (L1 <sub>2</sub> )	2.996141	1.183415	.836823	.334837
Ir <sub>3</sub> Zr (D0 <sub>3</sub> )	3.030435	1.155034	.798464	.334837
IrZr (L1 <sub>0</sub> )	3.118082	1.065320	.816067	.287301
IrZr (B2)	3.136023	1.051268	.824439	.287301
IrZr (B32)	3.113041	1.032941	.809960	.287301
IrZr <sub>3</sub> (L1 <sub>2</sub> )	3.259470	.943530	.769064	.239766
IrZr <sub>3</sub> (D0 <sub>3</sub> )	3.236335	.945095	.778761	.239766
NbZr <sub>3</sub> (L1 <sub>2</sub> )	3.352409	.882733	.722905	.066001
NbZr <sub>3</sub> (D0 <sub>3</sub> )	3.337626	.879449	.729566	.066001
NbZr (L1 <sub>0</sub> )	3.293732	.933753	.725154	-.060229
NbZr (B2)	3.278047	.929771	.734855	-.060229
NbZr (B32)	3.273462	.933422	.739348	-.060229
Nb <sub>3</sub> Zr (L1 <sub>2</sub> )	3.237312	.989477	.729573	-.186459
Nb <sub>3</sub> Zr (D0 <sub>3</sub> )	3.214737	.985204	.748261	-.186459
Ir <sub>2</sub> ZrNb (L1 <sub>2</sub> -like)	3.069983	1.107863	.804326	.161072
Ir <sub>2</sub> ZrNb (Huesler)	3.089152	1.107950	.810511	.161072
Ir <sub>2</sub> ZrNb (D0 <sub>3</sub> -like)	3.068522	1.104804	.807071	.161072
IrZr <sub>2</sub> Nb (L1 <sub>2</sub> -like)	3.204546	.997304	.770420	.113536
IrZr <sub>2</sub> Nb (Huesler)	3.189518	.993190	.784683	.113536
IrZr <sub>2</sub> Nb (D0 <sub>3</sub> -like)	3.179284	.997352	.782088	.113536
IrZrNb <sub>2</sub> (L1 <sub>2</sub> -like)	3.149602	1.046145	.775192	.792045
IrZrNb <sub>2</sub> (Huesler)	3.124752	1.052712	.785473	.792045
IrZrNb <sub>2</sub> (D0 <sub>3</sub> -like)	3.130798	1.051235	.792045	.792045

## Bibliography

- 1 V.L. Moruzzi, J.F. Janak, K. Schwarz, Phys. Rev. B, 37 (2), p. 790 (1988).
- 2 A.J. Freeman and Jaejun Yu, Alloy Phase Stability, 613-620, (1989).
- 3 H. L. Skriver, Phys. Rev. B, 31 (4), p. 1909 (1985).  
T. Hong, T.J. Watson-Yang, A.J. Freeman, T. Oguchi, Jian-Hua Xu, Phys. Rev. B, 41 (18), 12462 (1990).
- 4 A.J. Freeman, J.H. Xu, T. Hong, W. Lin, Ordered Intermetallics-Physical Metallurgy and Mechanical Behavior, Kluwer Academic Publications, 1992.
- 5 A.R. Williams, C.D. Gelatt, Jr., and V.L. Moruzzi, Phys. Rev. Letters, 44 (6), 429 (1980).
- 6 O. Gunnarsson, J. Harris, and R.O. Jones, J. Chem. Phys., 67, 3970 (1977).  
B.I. Dunlap, J.W.D. Connolly and J.R. Sabin, J. Chem. Phys., 71, 4993 (1979).
- 7 W. Kohn and L. J. Sham, Phys. Rev., 140, A1133 (1965).
- 8 P. Hohenberg, W. Kohn, Phys. Rev., 136, B864 (1964).
- 9 M. Schlüter and L.J. Sham, Phys. Today, 35, 36 (1982).
- 10 H.L. Skriver, The LMTO Method, Springer-Verlag, Berlin, 1984.
- 11 L. Kaufman and H. Nesor, Met. Trans., 5, 1623 (1974).  
L. Kaufman and H. Nesor, CALPHAD, 2, 337 (1978).
- 12 R. Kikuchi, Phys. Rev. 81, 988 (1951).
- 13 J.M. Sanchez and D. de Fontaine, Phys. Rev., B25, 1759 (1982).
- 14 C. Sigli and J.M. Sanchez, Acta. Met., Vol. 34, No. 6, pp. 1021-1028 (1986).
- 15 J.M. Sanchez, F. Ducastelle, and D. Gratias, Physica 128A, 334 (1984).
- 16 J.W.D. Connolly and A.R. Williams, Phys. Rev. B27, 5169 (1983).
- 17 J.M. Sanchez and J.D. Becker, Mat. Res. Soc. Symp. Proc., Vol. 291, p115 (1993)
- 18 J.M. Sanchez, Structural and Phase Stability of Alloys, J.L. Moran-Lopez, F. Mejia-Lira, J.M. Sanchez (editors), Plenum Press, NY, 1992, p. 151.
- 19 A.E. Carlsson and J.M. Sanchez, Solid State Comm., Vol. 65, No. 6, pp. 527-530 (1988).

- 20 N.C. Tso, J.M. Sanchez and J.K. Tien, Superalloys, Supercomposites and Superceramics, Academic Press, Inc., pp. 525-543 (1989).
- 21 R. Kikuchi, J.M. Sanchez, D. de Fontaine and Hisao Yamauchi, *Acta. Met.*, Vol. 28, pp. 651-662 (1979).
- 22 R. Kikuchi, *Acta Met.*, vol. 25, pp. 195-205 (1977).
- 23 Pearson's Handbook of Crystallographic Data for Intermetallic Phases, Vol. 3, 1985, ASM.
- 24 American Institute of Physics Handbook, 3rd ed., McGraw-Hill, NY, 1970.
- 25 T.B. Massalski, Binary Alloy Phase Diagrams, ASM, Metals Park, OH 1986, 1424 (Ir-Nb), 1441 (Ir-Zr), 1710 (Nb-Zr).
- 26 L. Topor and O.J. Kleppa, *J. Chem. Therm.*, 20, 1271 (1988).
- 27 D.A. Prokoshkin and E.V. Vasil'Eva, Alloys of Niobium, S. Monson, Jerusalem, 1965.
- 28 A.M. Gyurko and J.M. Sanchez, *Materials Science and Engineering*, A170, pp. 169-175 (1993)

## VITA

Gregory Allen Miller was born in Caracas, Venezuela on February 23, 1970 the second son of Jeanette Margaret Miller and Joe Oliver Miller. After growing up overseas, he found himself graduating from Plano East Senior High, Plano, Texas in 1988. He spent the next six years working towards and receiving a Bachelor of Science and Master of Science in Engineering from the University of Texas at Austin finishing in the spring of 1994. He currently resides in Austin, Texas.

Permanent Address: 147 Skyline Dr.  
Murphy, Texas 75094

This thesis was typed by Greg Miller.